during 2006 for comparison. Note that although the TRMM rainfall dataset begins in 1998, the long-term averages are taken from 1999 because extreme El Niño conditions in the first few months of 1998 distort the rainfall climatology in the SITCZ region.

Rainfall in the ITCZ is higher in the second 6 months of the year, and this climatological pattern was accentuated during 2006. Rainfall was lower than normal, particularly in February, and higher than normal in October through December 2006. This transition was also apparent in island rainfall records for the year. The islands of Micronesia in the western Pacific, which enter their dry season at the start of the calendar year, were very dry in some parts (e.g., the northern Marshall Islands) in the first quarter of 2006. South of the equator, rainfall in specific island groups was affected by the ENSO modulation of the SPCZ. The SPCZ was farther south than usual from January through May, as expected with La Niña, and farther north than usual in at least some months at the end of 2006 (e.g., December). However, in the area average of the SPCZ region plotted in Fig. 4.23, these local precipitation fluctuations average out and there is no marked pattern of precipitation anomalies through the year. As noted above, precipitation in the SITCZ region, which occurs mainly from February through April, was enhanced during 2006.

2) Atlantic ITCZ—A. B. Pezza and C. A. S. Coelho

The Atlantic ITCZ is a narrow but well-organized convective region that oscillates between several degrees north of the equator during July–November and only a few degrees south of the equator in January–May (Waliser and Gautier 1993). The ITCZ is active all year-round, demarcating the transition from the southeasterly to the northeasterly Atlantic trade winds. A zonally oriented cloud band is usually observed over the Atlantic Ocean basin extending from the northeast coast of South America to the northwest coast of Africa. Convective activity with high rainfall rates well inland is generally triggered by the nearby passage of the ITCZ as observed over northern Amazon in 2006 (Fig. 4.24).

The positioning of the ITCZ modulates the rainy season of northern/northeastern South America and northwestern Africa. Some regions experience a bimodal monthly rainfall distribution with two peaks—one when the ITCZ is moving southward and the other when it is moving back northward. Its seasonal migration and high asymmetry are primarily driven by land–sea temperature contrast, low-level winds, moisture convergence, and the meridional SST gradient between the North and the South Atlantic (Nobre and Shukla 1996). Large-scale dynamics given by Kelvin wave propagation affecting the Walker circulation can also drive the ITCZ's interannual variability, because ENSO is one of the relevant mechanisms of seasonal influences (Münnich and Neelin 2005).

High-resolution TRMM data indicate that during 2006 the ITCZ reached its southernmost position in April (2.5°S) and its northernmost position in August and September (10°N), and was to the north of its monthly climatological mean position during a number of months, particularly during the second half of the year. As a result, most of the tropical South Atlantic presented less rainfall in 2006 than the 1998–2005 annual mean value. However, the 2006 ITCZ's annual mean position appears close to its climatological annual mean due to a high variability, with outbursts of southward displacement from late austral summer to early austral winter. TRMM also shows a double ITCZ (Liu and Xie 2002) during April, with a primary band of convective clouds around 3°N across the entire equatorial Atlantic, and a secondary band of clouds around 2.5°S (Fig. 4.24).

April featured the interaction and organization of the secondary ITCZ branch with continental convection over northern Brazil, resulting in a wider ITCZ to the west of 30°W. This interaction over northern Brazil was also noted in May and June (Fig. 4.24), decaying in July. The ITCZ became less active from September to December, with little rainfall observed in September around 7.5°N in the central North Atlantic and near the African coast. August was the most active month for the period from July to December, when some areas near the African coast experienced high rainfall rates (Fig. 4.24). Interaction with western Africa rain was irregular during the year, with areas of positive and negative precipitation anomalies observed over the western tip of the continent. The onset of a weak El Niño event in the Pacific during mid-2006 contributed to keeping most of the ITCZ convective activity to the north of the equator for the remainder of the year, with annual rainfall below average over most tropical South Atlantic and above average over the tropical North Atlantic.

5. THE POLES—F. Fetterer, Ed.

a. Arctic—J. Richter-Menge, J. Overland, A. Proshutinsky, V. Romanovsky, R. Armstrong, J. Morison, S. Nghiem, N. Oberman, D. Perovich, I. Rigor, L. Bengtsson, R. Przybylak, A. Shiklomanov, D. Walker, and J. Walsh

1) Overview

The permanent presence of sea ice, ice sheets, and

continuous permafrost are unique features of the polar regions. The Arctic is further distinguished because it sustains a human population in a harsh environment. These characteristics amplify the impact of global climate change on both the regional physical and societal systems. These impacts reach beyond the Arctic region. For instance, studies are underway to determine the extent to which the loss of sea ice cover and the conversion of tundra to larger shrubs and wetlands, observed to have occurred over the last two decades, have impacted multiyear persistence in the surface temperature fields, especially in the Pacific sector. In this report, we provide observations that indicate continuing trends in the state of physical components of the Arctic system, including the atmosphere, ocean, sea ice cover, and land (Richter-Menge et al. 2006). The temporal extent of the data provides a multidecadal perspective and confirms the sensitivity of the Arctic to changes in the global climate system.

In 2006 there continues to be consistent signs of a general warming in the Arctic region, most apparent in the relatively small extent of the winter and summer sea ice cover and increased greenness of the tundra. However, there are also indications of a possible deceleration in the rate of change in some geophysical parameters, driven by pronounced shifts in atmospheric circulation patterns. These atmospheric circulation patterns mark a return to patterns that predominated prior to the mid-1990s. Perhaps correspondingly, the most recent observations indicate that the upper-ocean salinity and temperature in the vicinity of the North Pole and in the Beaufort Sea have relaxed toward the climatological norms reported since the 1950s. In 2006 ocean temperatures cooled in the Bering Sea and there was a slight recovery in the extent of the summer sea ice cover. The persistence and impact of the moderating 2006 conditions represents an intriguing and significant puzzle with respect to the contemporary global climate system.

2) Atmosphere

(i) Circulation regime

The annually averaged AO index in 2006 was slightly positive, continuing the trend of a relatively low and fluctuating index, which began in the mid-1990s (Fig. 5.1). This follows a strong, persistent positive pattern from 1989 to 1995. The current characteristics of the AO are more consistent with the characteristics of the period from the 1950s to the 1980s, when the AO switched frequently between positive and negative phases.

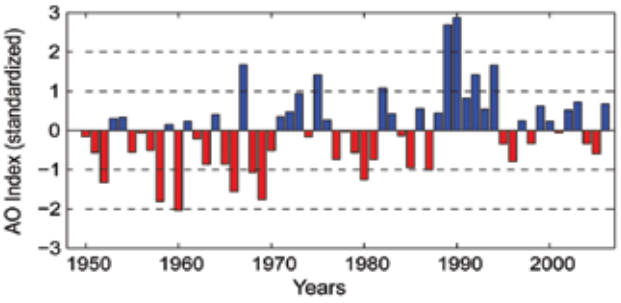

Fig. 5.1. Time series of the annually averaged AO index for the period 1950–2006 based on data available online (www.cpc.ncep.noaa.gov). [Source: I. Rigor.]

(ii) Surface temperatures and atmospheric circulation

In 2006, the annual surface temperature over land areas north of 60°N was 1.0°C above the mean value for the twentieth century (Fig. 5.2). The surface temperature in this region has been consistently above the mean since the early 1990s. Figure 5.2 also shows warm temperatures in the 1930s and early 1940s, possibly suggesting a longer-term oscillation in climate. However, a detailed analysis shows different proximate causes for the 1930s compared to recent maxima. The early warm and cold periods are associated with intrinsic variability in high-latitude circulation patterns; while the recent warm temperatures appear to have an anthropogenic component (Johannessen et al. 2004; Wang et al. 2007).

In 2006 the regional hot spot of 3°–4°C in springtime temperature anomalies observed during 2000–05 shifted from the western Arctic (east Siberia, Alaska, and surrounding waters) to the eastern Arctic (Svalbard and the Barents Sea) (Fig. 5.3). Despite

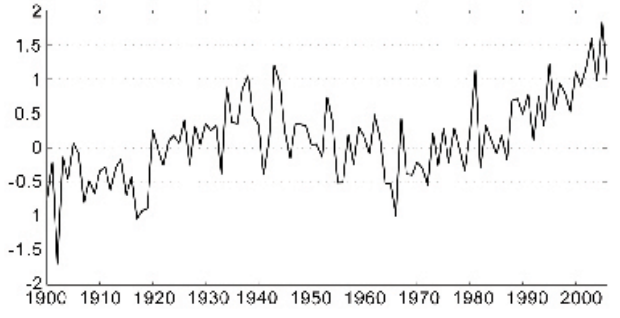

Fig. 5.2. Arctic-wide and annually averaged surface air temperature anomalies (°C; 60°N–90°) over land for 1900–2006 based on the CRU TEM2V monthly data set. Anomalies are relative to the twentieth-century average.

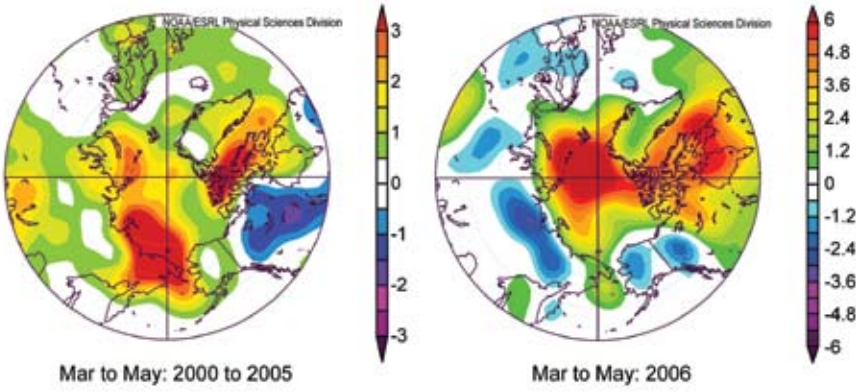

Fig. 5.3. Near-surface March–May temperature anomaly composites (at the 1,000 mb geopotential height level) for 2006 in contrast to 2000–05. While the entire Arctic remained warm, the hot spot shifted from the western to the eastern Arctic. The figure is based on NOAA National Centers for Environmental Prediction (NCEP) reanalysis fields via the Climate Diagnostics Center (www.cdc.noaa.gov). Anomalies are relative to a 1968–96 base period.

this shift, positive (warm) anomalies continue to remain over the entire Arctic. This pattern is in contrast to the North America/Eurasia dipole patterns of anomalies associated with the two principal atmospheric circulation features of the twentieth century, the Pacific North American Pattern and the Arctic Oscillation/Northern Annular Mode/North Atlantic Oscillation (Quadrelli and Wallace 2004; Overland and Wang 2005).

(iii) End of an era for the Bering Sea?

Air and ocean temperatures in the Bering Sea cooled significantly in 2006 from the previous six-year period of relatively warm temperatures (Fig. 5.4) and reduced sea ice cover (Fig. 5.10), in concert with Arctic-wide changes (Fig. 5.3). Vertically averaged temperatures from an oceanographic mooring on the southeastern Bering Sea continental shelf (Stabeno et al. 2002) recorded temperatures in 2000–05 that were 2°C warmer than earlier years, with 2005 as having the warmest summer. Winter 2006 was cold (note the drop in temperature between fall 2005 and summer 2006), with a –0.2°C air temperature anomaly recorded at St. Paul Island for November–April. Although winter 2006 was cold, the spring ocean temperatures and ice extent in 2006 were near their climatological averages because the beginning fall 2005 temperatures were warm. Temperatures in fall 2006, in contrast, started cold and the weather pattern for November–December 2006 was also cold, with a –1.0°C anomaly for November–December. The 6-year period of sustained warm temperatures (2000–05) was sufficient to restructure the ecosystem away from Arctic conditions that favored bottom species, to favoring midwater fishes (Grebmeier et al. 2006). Because of the dramatic shift in ocean and ice conditions in 2006 and the beginning of 2007, the future state of the Bering Sea ecosystem is now less certain.

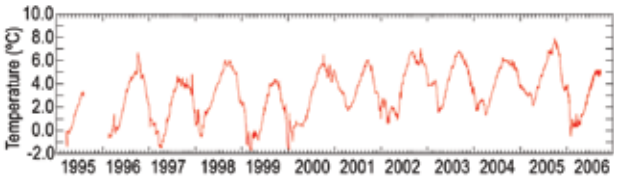

Fig. 5.4. Ocean temperatures (°C) from a mooring on the southeastern Bering Sea continental shelf.

3) Ocean

(i) Surface circulation regime

The circulation of the sea ice cover and ocean surface layer are closely coupled and are primarily wind driven. Data from satellites and drifting buoys indicate that the entire period of 2000–06 has been characterized by an anticyclonic circulation regime resulting from a higher sea level atmospheric pressure over the Beaufort Gyre, relative to the 1948–2005 mean, and the prevalence of anticyclonic winds. The sea surface atmospheric pressure at the North Pole together with the Arctic Oscillation index is a good indicator of the Arctic Ocean and atmosphere circulation regimes (Fig. 5.5). During high AO years, the low SLP dominates over the Arctic Ocean and the ice drift and ocean circulation are characterized by cyclonic (counterclockwise) motion. During low AO years, the high SLP prevails over the Arctic Ocean and sea ice and the ocean tends to circulate more in a clockwise sense. The dominance of the anticyclonic regime during the last decade of 1997–2006 is consistent with the AO index, which has exhibited relatively low and fluctuating values since 1996 (Fig. 5.5).

(ii) Heat and freshwater content

From 2000 to 2006, intensive investigations have been conducted in the vicinity of the North Pole (NPEO; online at http://psc.apl.washington.edu/northpole/) and in the western Arctic (BGOS; online at www.whoi.edu/beaufortgyre/index.html). Observations show that in the previous decade (1990s) the water temperature and salinity fields of the Arctic

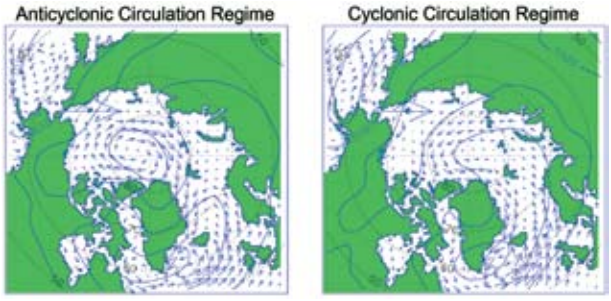

Fig. 5.5. Idealized patterns of the dominant wind-driven circulation regimes of the Arctic Ocean. Two circulation regimes of surface waters (anticyclonic: left; cyclonic: right) are shown in blue arrows. In the cyclonic regime the clockwise circulation pattern in the Beaufort Sea region (the Beaufort Gyre) weakens, and the flow across the basin, from the Siberian and Russian coasts to the Fram Strait (the Transpolar Drift), shifts poleward. The cyclonic pattern dominated during 1989–96; the anticyclonic pattern has prevailed since 1997. Sea level atmospheric pressure patterns are shown by lines (hPa) (adopted from Proshutinsky and Johnson 1997).

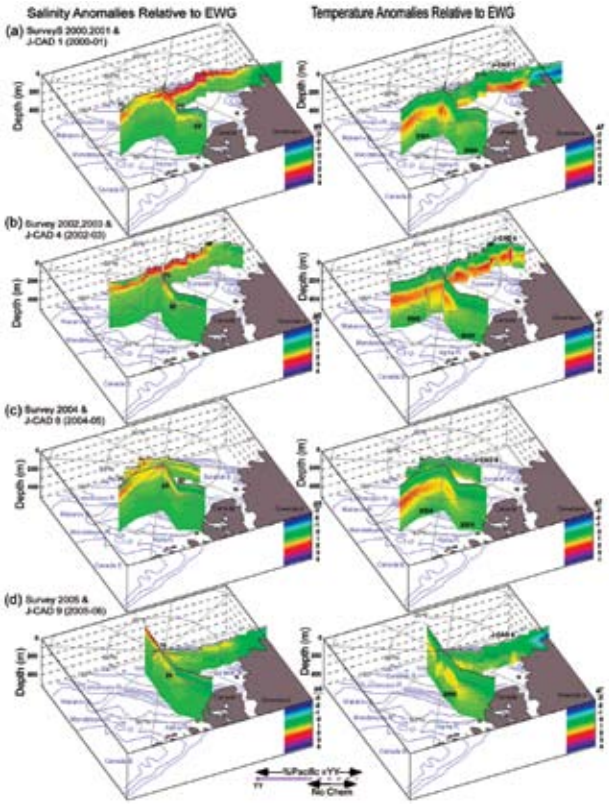

Fig. 5.6. (left) Salinity and (right) temperature anomalies relative to EWG climatology along the NPEO surveys and J-CAD tracks for the years indicated on the temperature sections. Gray vertical lines mark survey station sites. Deep magenta lines (left) mark location of greater than 20% Pacific-derived water at 100–150 m. Surface lines mark greater than 70% Pacific-derived water in the surface layer (from Morison et al. 2006a).

Ocean changed dramatically relative to the climatology of the Environmental Working Group atlas of the Arctic Ocean (Timokhov and Tanis 1997, 1998) where water temperature and salinity from observations were averaged and gridded for the decades of 1950, 1960, 1970, and 1980. Hydrographic data acquired at the North Pole in the 1990s show a strong increase in upper-ocean salinity and a large increase in Atlantic water temperature relative to EWG climatology average for all decades.

From 2000 to 2005, the oceanographic conditions in the North Pole region relaxed to near the pre-1990 climatology (Fig. 5.6). As characterized by average temperature and salinity anomalies relative to EWG climatology within 200 km of the North Pole, the change in the 1990s and the subsequent retreat to climatology are roughly consistent with a first-order response to the AO with a 5-year time constant and 3-year time delay (Morison et al. 2006a). Recent results indicate conditions in 2006 at the pole reverted to near 2004 conditions, but measurements of bottom pressure trends from 2002 to 2006 by GRACE suggest a return of oceanographic conditions over the entire Arctic Ocean to pre-1990s conditions (Morison et al. 2006b).

The western Arctic hydrography in the 1990s has also changed relative to climatology but, in opposition to the salinity increase at the North Pole, the salinity of the upper layer in the western Arctic was reduced. There are some indications that in the 2000s, relative to the 1990s, the salinity in this region has increased, but it is still significantly less than in EWG climatology. Since 2000, the temperature of the Pacific and Atlantic waters in the western Arctic is higher than in the 1990s and 0.8°–1.0°C higher than in EWG climatology.

The Beaufort Gyre is the major reservoir of freshwater in the Arctic Ocean. In 2000–06, the total freshwater content in the Beaufort Gyre has not changed dramatically relative to the climatology but there is a significant change in the freshwater distribution (Fig. 5.7, panels 3 and 4). The center of the freshwater maximum has shifted toward Canada and significantly intensified relative to the climatology. Significant changes were observed in the heat content of the Beaufort Gyre (Fig. 5.7, panels 1 and 2). It has increased relative to the climatology, primarily because of an approximately two-fold increase of the Atlantic layer water temperature (Shimada et al. 2004).

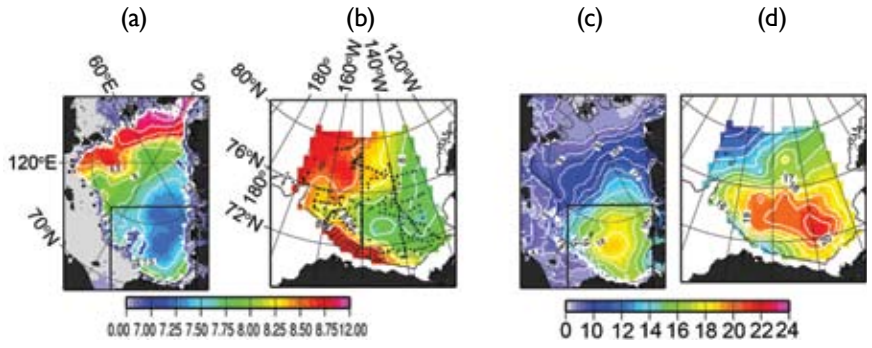

Fig. 5.7. (a),(b) Summer heat (10^{10} J m^{-2}) and (c),(d) freshwater (m) content. Panels (a) and (c) show heat and freshwater content in the Arctic Ocean based on 1980s climatology (Timokhov and Tanis 1997, 1998). Panels (b) and (d) show heat and freshwater content in the Beaufort Gyre in 2000–06 based on hydrographic surveys (black dots depict locations of hydrographic stations). For reference, this region is outlined in black in panels (a) and (c). The heat content is calculated relative to water temperature freezing point in the upper 1,000-m ocean layer. The freshwater content is calculated relative to a reference salinity of 34.8.

The Pacific water heat content in the Beaufort Gyre region has also increased, and it is possible that the pronounced sea ice reduction in this region, observed in 2006 (see Fig. 5.8, right panel), resulted from heat being released from this layer (Shimada et al. 2006). It is speculated that the major part of these changes in the freshwater and heat content occurred in the 1990s, but there are not enough data to confirm this.

(iii) Sea level

Figure 5.9 shows sea level time series from nine coastal stations in the Siberian Seas. These stations are still operational in the Arctic with data from 1954 to 2006. There is a positive sea level trend along the Arctic coastlines. Proshutinsky et al. (2004) estimated that for 1954–89 the rate of sea level rise along Arctic coastlines (40 stations), corrected for the GIA, was 0.185 cm yr^{-1}. For the nine stations shown in Fig. 5.9 the rate for 1954–89, after correction for their GIA, was 0.194 cm yr^{-1}. Addition of 1990–2006 data increases the estimated rate of increase in sea level, beginning in 1954, to 0.250 cm yr^{-1}. The sea level time series correlates relatively well with the AO index and with the inverse of the SLP at the North Pole. Consistent with these influences, sea level dropped significantly after 1990 and reached a minimum in 1996/97 when the circulation regime changed from cyclonic to anticyclonic. In contrast, from 1997 to 2006 the mean sea level has generally increased in spite of the more or less stable behavior of the AO and SLP. At this point, because of the large interannual variability, it is difficult to evaluate the significance of the change in

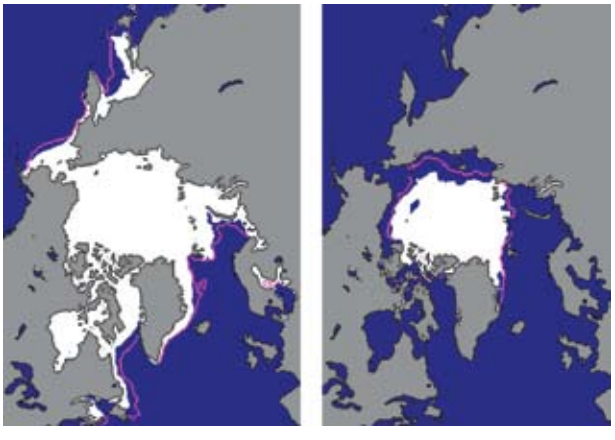

Fig. 5.8. Sea ice extent in (left) March and (right) September 2006, when the ice cover was at or near its maximum and minimum extent, respectively. The magenta line indicates the median maximum and minimum extent of the ice cover, for the period 1979–2000. The March 2006 maximum extent marked a record minimum for the period 1979–2006. (Figures from the Sea Ice Index, online at nsidc.org/data/seaice_index.)

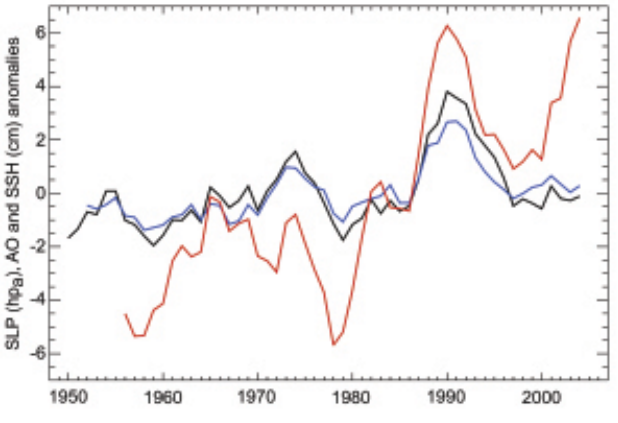

Fig. 5.9. Annual mean sea level at nine tide gauge stations located along the Kara, Laptev, east Siberian, and Chukchi Sea coastlines (red). The blue line is the 5-yr running mean anomalies of the annual mean AO index (blue) multiplied by three. The black line is the sea surface atmospheric pressure (SLP) at the North Pole (from the NCEP–NCAR reanalysis data) multiplied by –1.

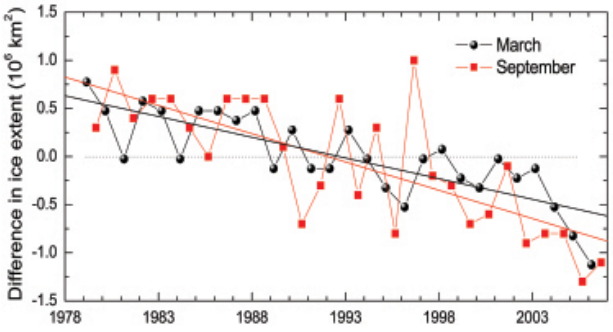

Fig. 5.10. Time series of the difference in ice extent in March (maximum) and September (minimum) from the mean values for the time period 1979–2006. Based on a least-squares linear regression, the rate of decrease in March and September was 2.5% decade^{-1} and 8.9% decade^{-1}, respectively.

relative trends.

4) Sea ice cover

(i) Extent and thickness

Satellite-based passive microwave images of the sea ice cover have provided a reliable tool for monitoring changes in the extent of the ice cover since 1979. During 2006, the minimum ice extent, typically observed in September, reached 5.9 million km^2 (Fig. 5.8, right panel). This marked a slight recovery from the record minimum of 5.6 million km^2 for the period 1979–2006, observed in 2005. Consistent with the past several years, the summer retreat of the ice cover was particularly pronounced along the Eurasian and North American coastlines. A unique feature was the isolated region of open water apparent in the Beaufort Sea.

The maximum ice extent, typically observed in March, was 14.4 million km^2 and set a record minimum for the period 1979–2006 (Fig. 5.8, left panel). It is notable that in March 2006 the ice extent fell within the mean contour at almost every location. In comparison, the mean ice extent for March and September, for the period 1979–2006, is 15.6 and 6.8 million km^2, respectively.

To put the 2006 minimum and maximum ice extent into context, the time series of the variability of ice extent in March and September for the period 1979–2006 are presented in Fig. 5.10. In both cases, a negative trend is apparent with a rate of 2.5% decade^{-1} for March and 8.9% per decade for September relative to the 1979 values. The summers of 2002–05 marked an unprecedented series of extreme summer ice extent minima (Stroeve et al. 2005).

Ice thickness is intrinsically more difficult to monitor. With satellite-based techniques (Laxon et al. 2003; Kwok et al. 2004) only recently introduced, observations have been spatially and temporally limited. Data from submarine-based observations indicate that the ice cover at the end of the melt season thinned by an average of 1.3 m between the period 1956–78 and the 1990s, from 3.1 to 1.8 m (Rothrock et al. 1999). Measurements of the seasonal ice cover do not indicate any statistically significant change in thickness in recent decades (Melling et al. 2005; Haas 2004; Polyakov et al. 2003).

(ii) Perennial and seasonal ice

The Arctic sea ice cover is composed of perennial ice (the ice located toward the center of the Arctic Basin that survives year-round) and seasonal ice (the ice around the periphery of the Arctic Basin that melts during the summer). Consistent with the diminishing trends in the extent and thickness of the cover is the observation of a significant loss of the older, thicker perennial ice in the Arctic (Fig. 5.11). Results from a simulation using drifting buoy data and satellite-derived ice concentration data to estimate the age distribution of ice in the Arctic Basin (Rigor and Wallace 2004) indicate that the March ice cover has experienced a significant decline in the relative amount of perennial ice over the period 1958–2006, from approximately 5.5 to 3.0 million km^2. While there is significant interannual variability, a general decrease in the amount of perennial ice appears beginning in the early 1970s. This trend appears to coincide with a general increase in the Arctic-wide, annually averaged surface air temperature, which also begins around 1970 (Fig. 5.2).

Results from a new technique employing data acquired by the NASA SeaWinds scatterometer on board the QuikSCAT have recently become available (Nghiem et al. 2005, 2006; Nghiem and Neumann 2007). In the half-decade of overlap, which begins in

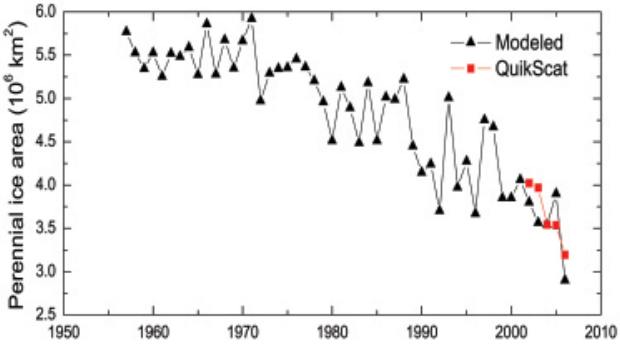

Fig. 5.11. Time series of area of perennial sea ice extent in March estimated by a drift age model and satellite-derived ice concentration data and observed by QuikSCAT within the drift age model domain.

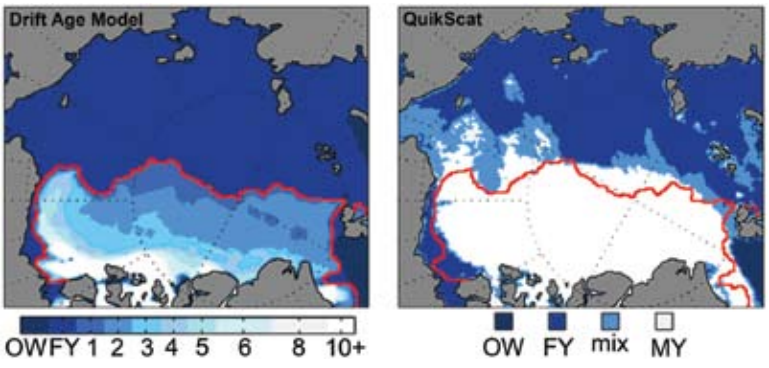

Fig. 5.12. Comparison of sea ice distribution estimated using the drift-age model (March average, left panel) with QSCAT observations (21 Mar 2006, right panel). The red line in both panels indicates ice age older than one year (i.e., perennial ice) as estimated by the drift-age model.

2002 and represents the period of data reprocessed to date by the QSCAT project, the two products provide consistent estimates of perennial ice in March and suggest a precipitous decrease in the perennial ice extent in the last few years.

Figure 5.12 presents a comparison of the ice distribution derived from the drift age model and observed by QSCAT in March 2006. The two products provide strikingly similar results. Both indicate that the older, thicker ice is concentrated in the western Arctic Basin. This result is consistent with the dominant ice circulation patterns in the Arctic (see Fig. 5.5). Ice residence times are typically longer in the western Arctic in the region of the Beaufort Gyre. The eastern Arctic is dominated by the Transpolar Drift, which carries sea ice out of the Arctic basin via the Fram Strait.

A relatively younger, thinner ice cover, similar to the one that has developed in recent years, is intrinsically more susceptible to persistent atmospheric or oceanic warming. It is of crucial importance to observe whether the sea ice cover will continue its decline or recover under the recent, more neutral AO conditions, which have shown to be more conducive to ice growth.

5) Land

(i) Vegetation

The most convincing evidence of widespread change of vegetation in the Arctic comes from trends in tundra greenness as detected by satellites. The NDVI is a measure of greenness derived from reflectance of the surface in the red and near-infrared channels. If the climate warms, higher NDVI values might be expected to shift northward. Earlier global studies of NDVI changes indicated a general pattern of increased NDVI in the region between 40° and 70°N during the period 1981–99 (Myneni et al. 1997, 1998; Zhou et al. 2001; Lucht et al. 2002). Studies of the NDVI in the tundra area of northern Alaska indicate an increase of 17% in NDVI values in this region where the SWI measured at ground stations across northern Alaska has been increasing by 0.16°–0.34°C yr^{-1} during the same period (Fig. 5.13) (Jia et al. 2003).

A more recent analysis indicates that different patterns of greening have occurred in the boreal forest and tundra areas of North America (Goetz et al. 2005). The NDVI has increased in tundra regions by an average of about 10% for all of North America, whereas the NDVI has declined in the boreal forest regions particularly during the past 10 years.

(ii) Permafrost

At the present time, there is no remote sensing

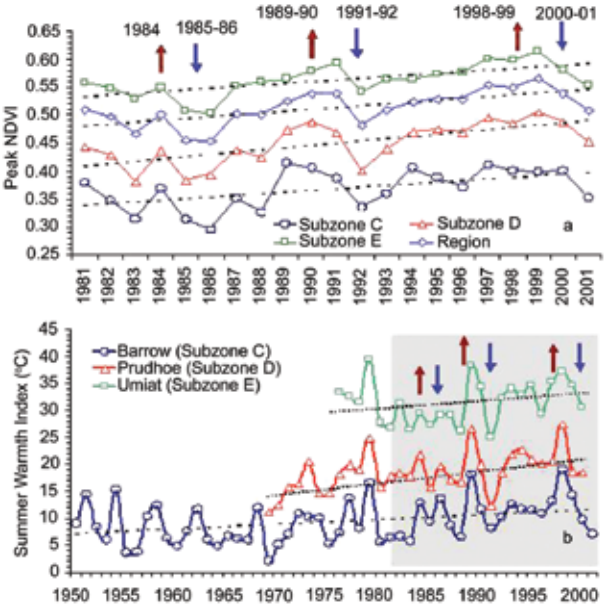

Fig. 5.13. (a) Time series of peak NDVI derived from 8-km-resolution AVHRR data from 1981 to 2001 for bioclimate subzones and for the whole Arctic slope. (b) SWI over the past 22–50 yr at meteorological stations in each bioclimate subzone. Dashed lines are linear regressions. The shaded area in (b) highlights the period of SWI covered by the NDVI data in (a). The arrows show years of corresponding increases (red) and decreases (blue) in NDVI and SWI. From Jia et al. (2003).

technique to remotely and extensively monitor permafrost temperatures. Long-term permafrost temperature data are available only from a few clusters of stations, mostly in North America. However, the situation could improve as a result of implementing an INPO, which is the major goal of the IPY TSP project. Observations from the long-term sites show a general increase in permafrost temperatures during the last several decades in Alaska (Osterkamp and Romanovsky 1999; Romanovsky et al. 2002; Osterkamp 2003), northwest Canada (Couture et al. 2003; Smith et al. 2003), Siberia (Pavlov 1994; Oberman and Mazhitova 2001; Romanovsky et al. 2002; Pavlov and Moskalenko 2002), and northern Europe (Isaksen et al. 2000; Harris and Haeberli 2003). Uninterrupted permafrost temperature records for more than a 20-year period have been obtained by the University of Alaska Fairbanks along the International Geosphere–Biosphere Programme Alaskan transect, which spans the entire continuous permafrost zone in the Alaskan Arctic. All of the observatories show a substantial warming during the last 20 years. This warming was different at different locations, but was typically from 0.5° to 2°C at the depth of zero seasonal temperature variations in permafrost (Osterkamp 2005). In 2006, there was practically no change to the mean annual temperatures at the permafrost surface if compared to 2005 (Romanovsky et al. 2006). These data also indicate that the increase in permafrost temperatures is not monotonic. During the observational period, relative cooling has occurred in the mid-1980s, in the early 1990s, and additionally in the early 2000s. As a result, permafrost temperatures at 20-m depth experienced stabilization and even a slight cooling during these periods.

Very similar permafrost temperature dynamics were observed in the European north of Russia during the same period (Fig. 5.14). However, there is some lag in the soil temperature variations at the Alaskan sites compared to the Russian sites. This observation is similar to what was discovered in comparison with permafrost temperature dynamics in Fairbanks, Alaska, and Yakutsk, Russia (Romanovsky et al. 2007). Relative cooling has occurred in the Vorkuta region in the early and late 1980s and then in the late 1990s. The total warming since 1980 was almost 2°C at the Vorkuta site.

Data on changes in the ALT in the Arctic lowlands are less conclusive. In the North American Arctic, ALT experiences a large interannual variability, with no discernible trends. This is likely due to the short length of historical data records (Brown et al. 2000). A noticeable increase in the active layer thickness was reported for the Mackenzie Valley (Nixon et al. 2003). However, this positive trend was reversed into a negative trend at most of these sites after 1998 (Tarnocai et al. 2004). An increase in thickness of more than 20 cm between the mid-1950s and 1990 derived from historical data collected at the Russian meteorological stations was reported for the continuous permafrost regions of the Russian Arctic (Frauenfeld et al. 2004; T. Zhang et al. 2005). At the same time, reports from several specialized permafrost research sites in central Yakutia show no significant changes in the active layer thickness (Varlamov et al. 2001; Varlamov 2003). The active layer was especially deep in 2005 in interior Alaska. Around Fairbanks the 2005 active layer depth was the deepest observed in the past 10 years. Data from many of these sites show that the active layer developed during the summer of 2004 (one of the warmest summers in Fairbanks on record) and did not completely freeze during the 2004/05 winter. A thin layer just above the permafrost table was unfrozen during the entire winter. The active layer in the summer of 2006 was also one of the deepest on record at most of the observation sites in the Fairbanks area, even though the summer air temperatures were close to normal.

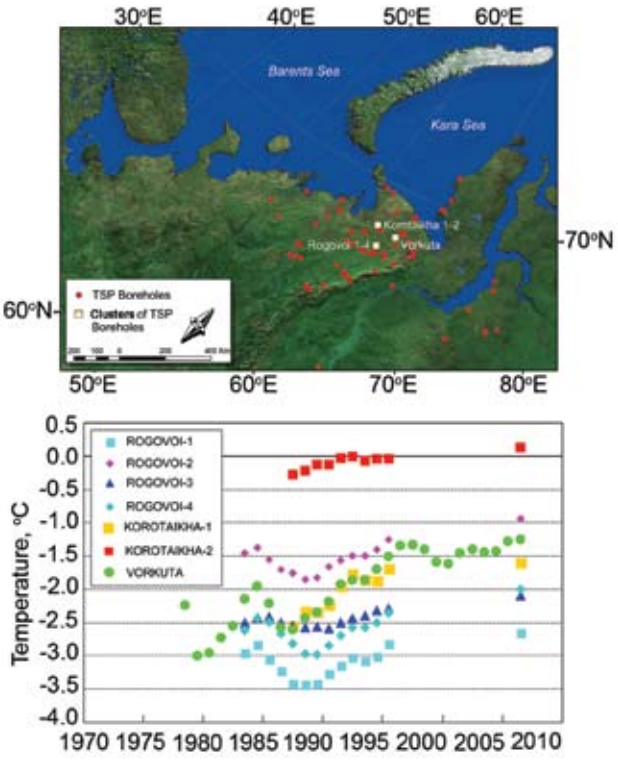

Fig. 5.14. Top: Location of the long-term MIREKO permafrost observatories in northern Russia. Bottom: Changes in permafrost temperatures at 15-m depth during the last 20–25 yr (Oberman 2007).

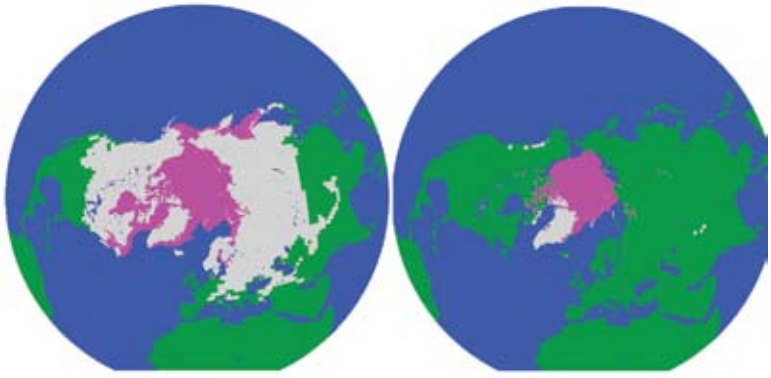

Fig. 5.15. Mean snow cover extent (gray), 1966–2006, for (left) February and (right) August from the Northern Hemisphere EASE-Grid Weekly Snow Cover and Sea Ice Extent dataset (Armstrong and Brodzik 2005). The product includes climatologies of snow average conditions, probability of occurrence, and variance based on NOAA charts as revised by Robinson et al. (1993).

(iii) Snow extent

As dicussed in section 2c(2), NOAA has produced snow extent charts since 1966 (Robinson et al. 1993; Frei and Robinson 1999). These charts were primarily derived from the manual interpretation of visible band imagery until 1999, when passive microwave and other data sources became available (Ramsay 1998; NOAA/NESDIS/OSDPD/SSD 2004, update 2006). Passive microwave data can enhance snow measurements based on visible data alone, sensing the surface through clouds and in darkness. However, passive microwave may not detect some areas of shallow snow that can be seen in visible band imagery. As a result, time series from the two sources can differ. Figure 5.15 shows mean snow cover for the 1966–2006 period. Figure 5.16 compares a microwave data–derived snow cover dataset (Armstrong and Brodzik 2001; Armstrong et al. 2005b) with NOAA snow extent data. Both show similar interannual variability and consistently indicate Northern Hemisphere maximum extents exceeding 40 million km^2. The NOAA time series indicates a decreasing trend of –2.0% decade^{-1} (Brodzik et al. 2006). There is a decreasing trend of –0.7% decade^{-1} in the microwave snow cover, although it is not significant at the 90% level. Both sources indicate a decreasing trend in snow cover in every month but November and December. The strongest seasonal signal occurs during May–August when both indicate significant decreasing trends. The western United States is among the regions with the strongest decreasing trends, supporting Groisman et al. (2004) and Mote et al. (2005) results using in situ observations. Shallow snow cover at low elevations in temperate regions is the most sensitive to temperature fluctuations and hence most likely to decline with increasing temperatures (IPCC 2007).

(iv) Glaciers

Glaciers and ice caps, excluding those adjacent to the large ice sheets of Greenland and Antarctica, can be found on all continents except Australia and have an estimated area between 512 and 540 × 103 km^2. The complicated and uncertain processes that control how fast glaciers move make it difficult to use changes in the areal extent of glaciers as a straightforward indicator of changes in climatic conditions. Further, many large collections of glacier photographs are available, but it is only in the last decade or so that remote sensing imagery has provided a means to monitor changes in the areal extent of glaciers. The Global Land Ice Measurements from Space glacier database project, with participation from more than 60 institutions in 28 nations, is working now on a baseline study to quantify the areal extent of existing glaciers (Armstrong et al. 2005a)

Mass balance measurements, or the difference between the accumulation and ablation, are a more direct method to determine the year-to-year "health" of a glacier. Changes in mass balance correspond to changes in glacier volume. These measurements are typically obtained from less than about 0.2% of the

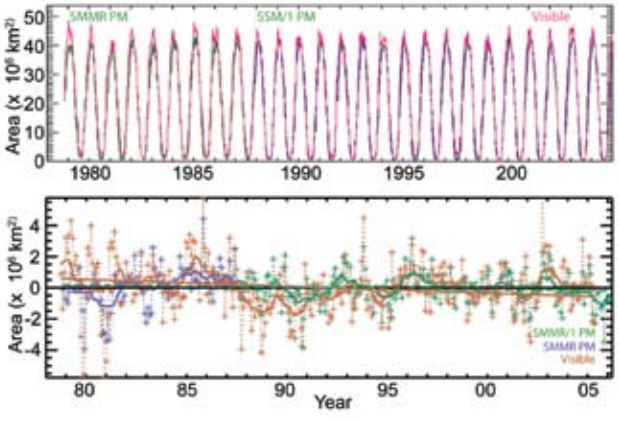

Fig. 5.16. Time series of Northern Hemisphere SCA derived from passive microwave (green/blue) and visible (pink) sensors (top), and SCA departures from monthly means (bottom), from NOAA snow charts (orange) and microwave (purple/green) datasets.

world's glaciers. Researchers have measured mass balance on more than 300 glaciers since 1946, although a continuous record exists for only about 40 glaciers since the early 1960s. Nevertheless, considerable compilation and analysis has occurred (e.g., Cogley 2005). These results indicate that in most regions of the world, glaciers are shrinking in mass. From 1961 to 2003, the thickness of "small" glaciers decreased approximately 8 m, or the equivalent of more than 6,000 km^3 of water (see http://nsidc.org/sotc/glacier_balance.html). Recent mass loss of glaciers and ice caps is estimated to be 0.51 ±0.32 mm SLE per year between 1961 and 2003 and 0.81 ±0.43 mm SLE per year between 1993 and 2003 (Dyurgerov and Meier 2006; online at http://nsidc.org/sotc/sea_level.html). The greatest mass losses per unit area are found in Patagonia, Alaska, and the northwest United States/southwest Canada. However, because of the corresponding large areas, the biggest contributions in total to sea level rise come from Alaska, the Arctic and the Asian high mountains.

(v) River discharge

The river discharge database R-ArcticNet (available online at www.R-Arcticnet.sr.unh.edu) was extended up to 2004 for 48 downstream river gauges. The last five years were characterized by an increase of total discharge to the Arctic Ocean mainly due to a contribution from Asian rivers. Mean 2000–04 discharge from Asia was 110 km^3 (5%) higher than over the previous 20 years. The mean discharge to the ocean from North America and Europe for 2000–04 was practically unchanged relative to 1980–99. A consistent increase in river discharge is observed from Eurasia for a longer time interval as well. Mean discharge over 2000–04 for the large Eurasian rivers was 3%–9% higher than the discharge over 1936–2004. Thus, the contemporary data further confirms the presence of a significant increasing trend in the freshwater discharge to the Arctic Ocean from Eurasia documented earlier by Peterson et al. (2002). The maximum total discharge of the six largest Eurasian rivers over 1936–2004 was observed in 2002, at 2080 km^3 yr^{-1}.

b. Antarctic

1) Overview—T. Scambos

The Antarctic climate pattern and mean circulation is stabilized by the presence of the encircling Southern Ocean (for discussion here, the portions of the major oceans south of 50°S; definitions vary), and by the huge, roughly pole-centered ice plateau of the Antarctic continent. It is characterized by intense eastward-moving polar cyclonic systems and strong off-continent katabatic flow. Nevertheless, it is also strongly influenced by climate patterns to the north (e.g., ENSO; Bromwich et al. 2004a; Turner 2004), and it exhibits large circulation shifts that are correlated with changes to these broad temperate and tropical patterns. These changes in the atmospheric circulation in turn influence the formation and drift of Antarctic sea ice. The Southern Ocean sea ice cycle represents the third-largest annual change of the Earth's surface (after Northern Hemisphere leaf out, and seasonal northern snow cover), and its growth and retreat has a very large influence on heat and moisture transport to the atmosphere, as well as on the southern oceanic ecosystem.

The year 2006 continued the recent trend of warming in the peninsula and offshore west Antarctica, and a trend of moderate and shorter-duration anomalies in the SAM circulation index (Figs. 5.17 and 5.18). While annual averages for the high southern latitudes showed broad patterns of mildly warmer-than-average conditions, there were several anecdotal indications of a cool austral winter in 2006 (snow in South Africa; iceberg remnants off southern New Zealand). The annual mean SAM index was weakly positive, but there were several significant circulation shifts during the year. Sea ice trends were remarkable in that the year included both the record minimum and record maximum ice extents relative to the 1979–2006 period (the period of accurate satellite observations), possibly linked to the shifts in circulation pattern during the ice growth period. The extent of seasonal melt during the 2005/06 spring–summer period was quite low overall, but included an anomalously long melt event for the northeastern

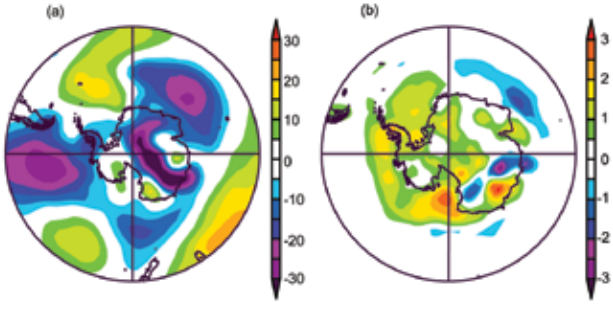

Fig. 5.17. (left) Annual anomaly of 850-hPa geopotential height and (right) surface temperature for 2006 relative to the 1979–2005 period, from NCEP–NCAR reanalysis data. The 850-hPa value is inferred for high-altitude regions of the continent; however, this level best illustrates the near-surface and middle-troposphere patterns. [Source: NOAA/ESRL, generated online at www.cdc.noaa.gov.]

Ross Ice Shelf and Shirase Coast. While springtime ozone depletion reached record proportions by a small margin, it is still anticipated that detectable decreases in springtime ozone loss will occur by 2023.

2) Atmospheric circulation—R. L. Fogt, D. H. Bromwich, J. Turner, and S. Barreira

The year 2006 was dominated by strong changes in circulation reflecting changes in the SAM and the zonal wavenumber-3 pattern (Figs. 5.18 and 5.19). Here, the SAM index is based on the definition from the CPC (see www.cpc.noaa.gov/products/precip/CWlink/daily_ao_index/aao/aao.shtml) as the leading EOF of 700-hPa geopotential height anomalies south of 20°S. The year 2006 showed several significant SAM anomalies, particularly in May and August, when the SAM was more than one standard deviation above, and two standard deviations below, its 1979–2005 mean, respectively (Fig. 5.18). Overall, the year showed a mildly positive SAM index, continuing a trend toward positive mean SAM over the past several decades (Fig. 5.18, inset).

Based on an examination of monthly mean patterns, we divided the Antarctic 2006 climate into five multimonth periods (Fig. 5.18, top), and in Fig. 5.19 we examine their 850-hPa height and surface temperature anomalies. Strong geopotential height and pressure decreases across Antarctica, and corresponding rises in the southern midlatitudes, are seen for the May–June–July period (Fig. 5.19e), in association with the positive SAM index noted above. This led to warmer-than-average temperatures in the Weddell Sea by up to 6°C (Fig. 5.19f); and cooler temperatures over offshore Dronning Maud Land and Enderby Land (0°–60°E), again by 6°C. An abrupt shift to nearly opposite conditions, with opposing-sign temperature anomalies, occurred during the August–Sep-

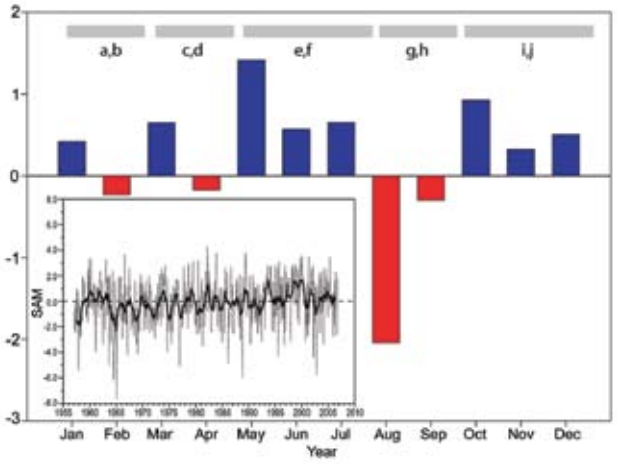

Fig. 5.18. Monthly standard deviations of the SAM for 2006 relative to the 1979–2005 mean. Along the top, the periods of distinctive climate patterns examined in Fig. 5.19 are shown. Inset: Trends in monthly mean SAM index (dashed line) and running 12-month mean SAM, 1957–2006, from www.nerc-bas.ac.uk/icd/gjma/sam.html.

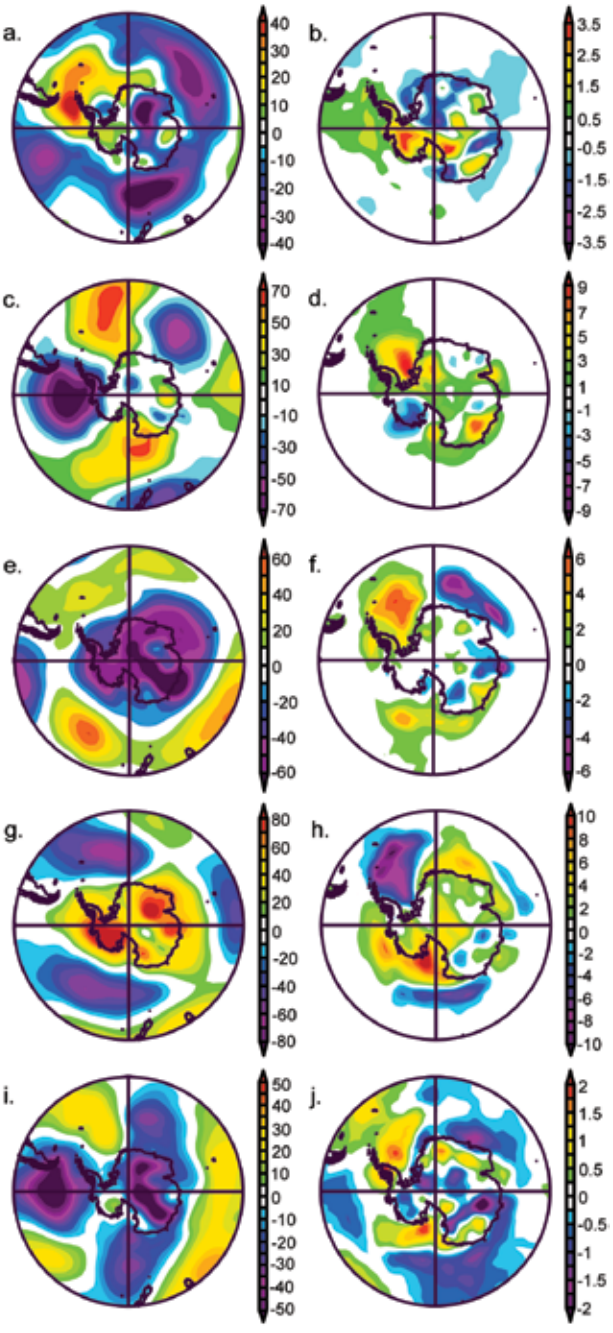

Fig. 5.19. (left) 850-hPa geopotential height anomaly and (right) surface temperature anomaly (°C) relative to 1979–2005 climatology for five distinctive periods in 2006.

tember period (Fig. 5.19h). This period also showed intensely warm conditions (up to 10°C above mean) for the eastern Ross Sea and Ross Ice Shelf area.

The SAM has been characterized by high month-to-month variability since 2003. Notably, December 2006 initiated a mild El Niño event, which tends to produce positive height/pressure anomalies in the Amundsen–Bellingshausen Seas. However, Fig. 5.19i shows that a negative height anomaly was observed in this region during October–December, which suggests there was no significant climate teleconnection to the South Pacific from the late-onset 2006 El Niño at that time.

3) Surface and radiosonde observations—N. Adams, J. Turner, and T. Scambos

The patterns of circulation and temperature had a concurrent effect on surface weather observations during 2006 (Fig. 5.20). At the Australian bases [Casey (66.28°S, 110.52°E), Davis (68.58°S, 77.97°E), and Mawson (67.60°S, 62.87°E)], the large change in circulation and SAM index that occurred between July and August, and again between September and October, is clearly reflected in mean surface pressure anomaly shifts at those times. Temperature anomalies (warm in March–April, cooler generally in May–July) for the east Antarctic bases concur with the regional plots shown in Fig. 5.19. In the northeastern peninsula, surface observations from a number of stations operated by Argentina (Skvarca et al. 2006) indicate a very warm 2005/06 austral summer period, among the warmest during the preceding 30 years, during which extensive melt and melt ponding was observed. However, temperatures for the western peninsula were only slightly greater than the mean.

The long-term radiosonde record from these stations and several others has indicated that a midtropospheric, winter season warming has been taking place above the Antarctic in recent decades (Turner et al. 2006). At Syowa station on the coast of east Antarctica, temperatures at the 500-hPa level have risen by 0.7°C decade^{-1} over the last 30 years. During 2006, however, the winter 500-hPa temperatures at Syowa were below average after near-record warm temperatures in 2005, 2003, and 2002.

4) Surface mass balance—A. Monaghan and D. Bromwich

Snowfall accumulation is the mass input to the Antarctic ice sheets, and is the net result of precipitation, sublimation/vapor deposition, drifting snow processes, and melt (Bromwich 1988). Of these, precipitation (almost entirely in the form of snowfall) is the dominant term of surface mass balance at regional and larger scales (Genthon 2004); only in relatively limited areas does ablation equal or exceed snow input, although recent remote sensing analyses suggest these may be more widespread than previously thought (firn "glaze" areas of near-zero accumulation; Scambos et al. 2006). Atmospheric models have been the primary means of assessing the variability of Antarctic snowfall for periods longer than a decade (e.g., Bromwich et al. 2004b). More recently, satellite radar altimetry (e.g., Davis et al. 2005) and

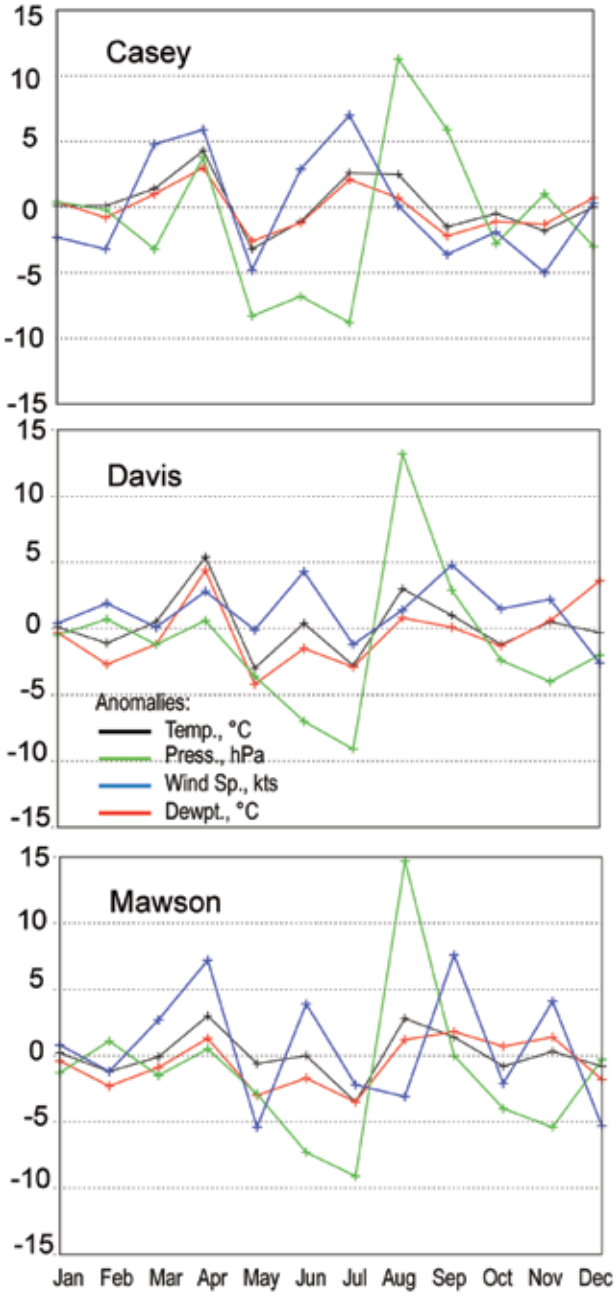

Fig. 5.20. Monthly mean weather anomalies for the Australian Antarctic stations Casey, Davis, and Mawson.

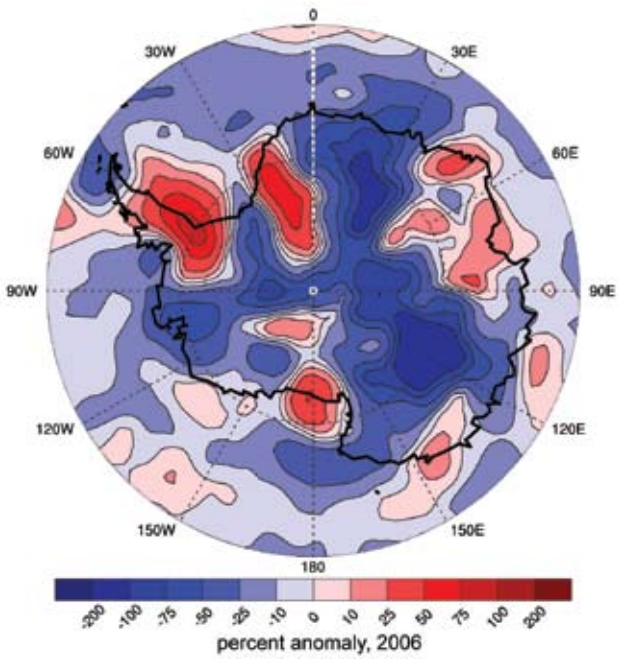

FIG. 5.21. Detrended precipitation anomalies (% yr^{-1}) from NN2 for 2006 compared with the 1979–2006 mean.

other satellite-based techniques (e.g., Velicogna and Wahr 2006) are increasingly being used to study surface and total ice sheet mass balance for periods of < 1 decade. The most recent model studies and observational data indicate there has been no trend in snowfall in recent decades (Van de Berg et al. 2005; Monaghan et al. 2006).

Precipitation fields from the NOAA/NWS/NCEP/DOE Reanalysis II (NN2; a successor to the NCEP–NCAR Reanalysis) are employed here to assess Antarctic snowfall for 2006. In recent studies (e.g., Bromwich et al. 2004b), snowfall trends in NN2 have been found to have an anomalous upward trend from 1979 onward, compared to other model-based records, snowstake measurements, and ice core records; however, the interannual variability of the snowfall is in very good agreement with other models (Monaghan et al. 2006). Therefore, a detrended NN2 record (linear mean trend subtracted) roughly approximates the "flat" trends that more accurate models predict. Using this we calculate a 2006 snowfall anomaly pattern compared to the 1979–2006 mean (Fig. 5.21).

In general, the anomaly over the continent interior is negative, and is positive over most of the Antarctic Peninsula and western Weddell Sea. Smaller positive trends over the Amery and northern Ross Ice Shelves suggest that the mean wavenumber-3 pattern (Fig. 5.17a) had a strong impact on precipitation. While the pattern of precipitation anomaly and circulation anomaly are consistent with a mildly positive SAM for 2006, the link between the SAM and precipitation is not as robust as the link for temperature (Genthon et al. 2003). Continentwide, the mean anomaly is small (–6%), with no month exceeding two standard deviations from the mean. The observed downward fluctuation would contribute an increase to sea level of approximately 0.30 mm for the year.

5) Sea ice extent and concentration—R. Massom, S. Barreira, and T. Scambos

Sea ice extent anomalies varied widely during the year, from record-low January and March extent (March was –18% relative to the 1979–2006 mean) to record highs of +4% for September and October, based upon analysis of monthly mean SSM/I-derived sea ice concentration data produced by the NSIDC

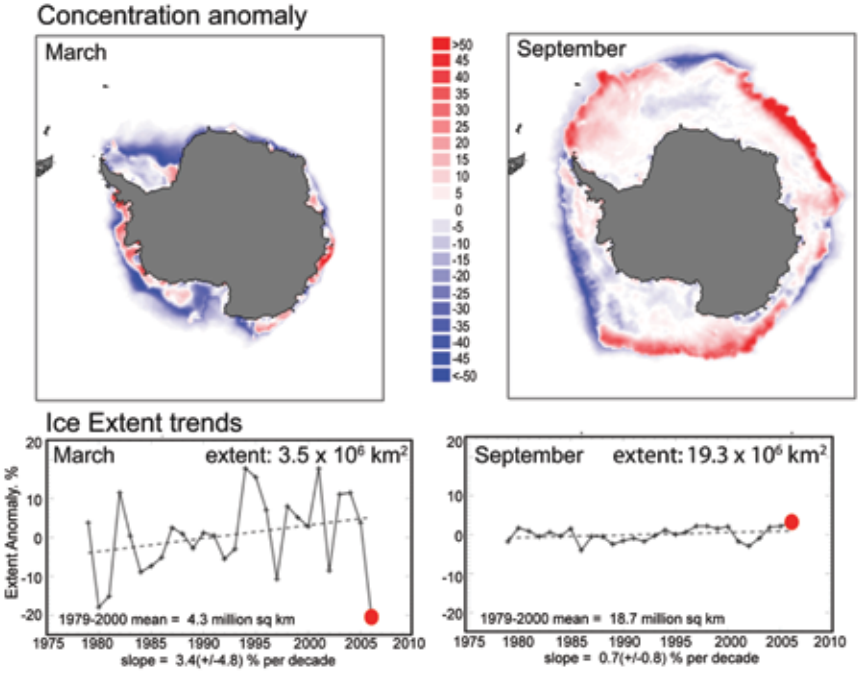

FIG. 5.22. (top) Sea ice concentration anomaly (%) for March and September, 2006, and (bottom) trends in sea ice extent.

Sea Ice Index project (Fig. 5.22; see Fetterer and Knowles 2004). However, by December 2006, sea ice extent was below average again. Strong regional variability is also apparent in ice extent and concentration anomalies. For the austral sea ice minimum period (February–March), the record low is primarily a result of greater-than-average March retreat in the Weddell Sea. This is likely a result of the intense warmth (up to 5°C above average) in the eastern Weddell in March, and a circulation pattern that favored southward and eastward wind-driven drift of the pack. In the autumn growth season, positive anomalies in the Amundsen Sea and western Indian Ocean sectors are balanced by negative anomalies in the South Atlantic (Weddell Sea) and Ross Sea/WPO sectors. The winter ice cover in August is characterized by major negative anomalies (indicative of wind-driven ice compaction) in the Bellingshausen–Amundsen Seas plus WPO sectors and a lesser negative anomaly skirting the Greenwich meridian. These are counterbalanced by equally large positive anomalies in the Weddell Sea, Ross Sea, and Indian Ocean sectors. This pattern persisted through September–October. In fact, the Indian Ocean sector experienced large positive extent and concentration anomalies from April through November. Locations of extent anomalies, and the overall record extent during the winter maximum, suggest an influence from the earlier positive SAM mode and strong positive wavenumber-3 anomaly, and the presence of lower-than-average temperatures near the winter ice edge (see Massom et al. 2006; Raphael 2004).

6) Seasonal melt extent and duration—H. Liu, Lei Wang, and K. Jezek

The extent, onset date, end date, and duration of snowmelt on the Antarctic Ice Sheet during the 2005/06 austral summer, and a time series spanning 1979/80 to the 2003/04 summers, have been derived using passive microwave remote sensing (Liu et al. 2005). The 25 season mean melt extent is 1.277 million km^2, or 9.34% of the continent's area. During the 2005/06 summer, melt extent, including all areas with at least one day of surface melting, was 1.009 million km^2, or 7.4% of the continent (Fig. 5.23). This is the second lowest extent during this period, after 1999/2000 (Liu et al. 2006). The 2005/06 melt season extended from 5 November to 4 March. Peak melt extent occurred on 7 January.

Extensive and continuous melt occurred on the ice shelves of the Antarctic Peninsula, and the Amery, Abbot, West, and Shackleton Ice Shelves. Melt areas are also scattered along the coasts of Wilkes Land and in glacial valleys in the Transantarctic Mountains. A brief but extensive surface melting occurred over the west Antarctic ice streams and Ross Ice Shelf in mid-December and again in January, coinciding with warm air temperature anomalies there during this time (Fig. 5.19b). Regionally, 2005/06 was a normal melt year for the Antarctic Peninsula, Amery Ice Shelf, Shackleton Ice Shelf, and West Ice Shelf, an extremely high melt year for the Ross Ice Shelf and Abbot Ice Shelf, and an extremely low melt year for the Ronne–Filchner Ice Shelf, and the ice shelves along the Queen Maud Land and Wilkes Land coasts.

7) 2006 austral springtime ozone depletion—P. A. Newman, B. J. Johnson, D. Lubin, S. J. Oltmans, and R. C. Schnell

Springtime ozone depletion in 2006 was by a small margin the most severe ever recorded as measured from the NASA Aura satellite's OMI. The ozone hole's area had an average late-September extent of 27.4 million km^2 (Fig. 5.24). The ozone hole area is estimated by integrating the area of observations with total ozone values less than 220 DU from the NASA TOMS instruments and the Aura OMI satellite instrument. A record-minimum column ozone abundance of 85 DU was recorded on 8 October over east Antarctica. This is consistent with the extremely cold temperatures in that same altitude range during this period (~ –85°C), which led to extensive PSC formation. Aura MLS observations revealed high ClO abundances (> 1 ppbv) filling nearly all of the polar

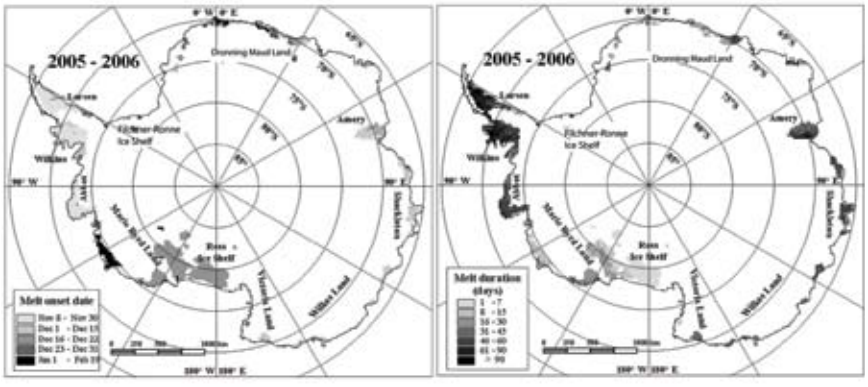

Fig. 5.23. Melt onset date and melt season duration in days, for the 2005/06 melt season.

vortex. While the 2006 ozone depletion was severe, it began about two weeks later than the mean of those years with comparable severity (Fig. 5.24a).

Information on the vertical structure of the ozone hole is provided by the NOAA/Earth System Research Laboratory Global Monitoring Division balloon-borne ozonesonde measurements (71 launches) at the Amundsen-Scott South Pole Station in Fig. 5.25. The total column of O_3 (blue line) is in Dobson units (and the 20–24-km stratospheric temperature (red line) illustrates the development of the O_3 hole over South Pole Station in 2006. The severity of O_3 depletion depends on wintertime stratospheric temperatures, the stability of the polar vortex, and active chlorine levels. The 2006 measurements showed some of the lowest O_3 amounts ever in the 21-year record at South Pole. Average total column of O_3 was 270 DU in July through mid-August before stratospheric O_3 began the now-typical, steady decline throughout September. Stratospheric temperatures remained colder than normal during that month. The total O_3 minimum of 93 DU at the South Pole (shown in Fig. 5.25c) was measured on 9 October, consistent with the satellite observations. This low value occurred about one week later than normal, and was the third lowest minimum observed since South Pole measurements began in 1986. The depletion was the largest ever observed within the primary O_3 layer from 14 to 21 km, dropping from 125 DU in late July to a record low of 1.2 DU (99% depletion) in early October. The polar vortex remained stable over the Antarctic for the final weeks of 2006, resulting in a slow recovery in stratospheric O_3. Significant amounts of ozone-enriched air transported from midlatitudes eventually reached the South Pole on 8 December, as shown in Fig. 5.25a and 5.25d, when total O_3 increased to 301 DU.

Despite its severity, the 2006 event does not necessarily signify a worsening of polar ozone depletion. Ozone depletion over Antarctica is highly sensitive to the dynamics of the winter stratospheric polar vortex, and this dynamical variability has yielded significant interannual variability in springtime ozone depletion over the past decade. For example, the weak and split polar vortex of 2002, accompanied by an anomalously warm stratosphere, led to a very mild springtime ozone depletion. During 2006, the polar vortex was much colder than average. These colder temperatures resulted from a weaker tropospheric planetary wave–driven warming of the stratosphere during the July–September period (related to the positive anomaly in 850-hPa level in Fig. 5.19g). Given these conditions, the severe 2006 ozone depletion is consistent with the decadally averaged abundance of anthropogenic ODS (mainly chlorofluorocarbons). ODS abundances have only recently started to decline in response to the Montreal Protocol; the rate of this decline is ~0.6% year^{-1}, not yet enough to reduce the severity of the springtime ozone depletion over Antarctica. According to models by Newman et al. (2006), ODS mitigation resulting from the Montreal Protocol should yield a

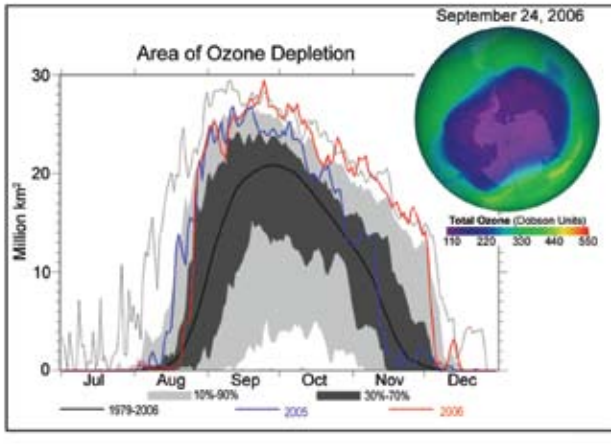

Fig. 5.24. Ozone depletion for austral springtime period at South Pole, 2006 (red), 2005 (blue), maximum over the period 1979–2005 (gray line), and the climatological mean (black), with extent of ozone depletion as of 24 Sep 2006, the maximum area ever recorded (inset).

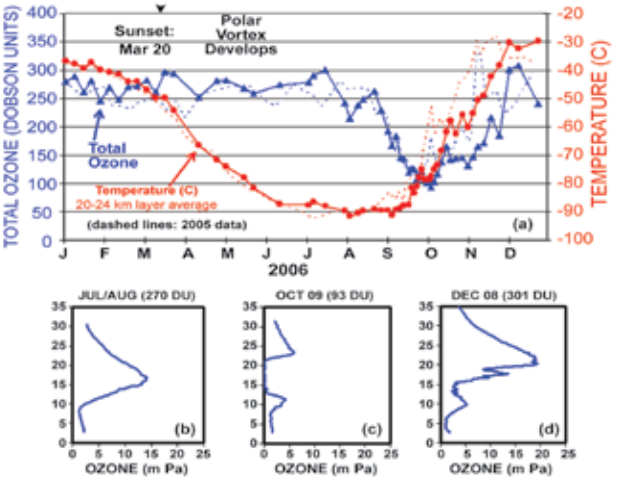

Fig. 5.25. (a) Summary of South Pole total ozone in DU and stratospheric temperatures measured by ozonesondes during 2006. Dashed lines show the respective 2005 data. Three selected profiles of altitude versus ozone partial pressure (millipascals) are shown in the lower panels: (b)the July through mid-August average profile prior to the 2006 ozone hole, (c) the minimum total ozone, and (d) the postozone hole. [Source: B. Johnson and S. Oltmans, NOAA/ESRL/GMD.]

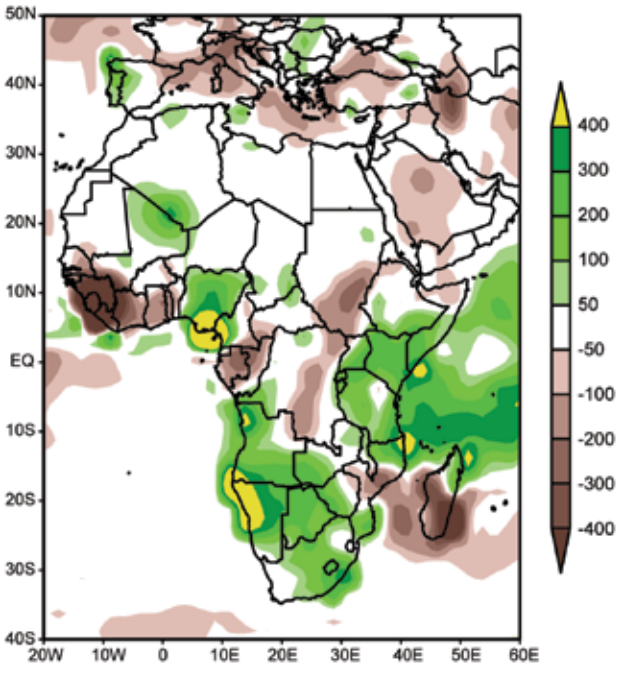

Fig. 6.1. African 2006 annual precipitation anomalies (mm; 1979–2000 base) from the CAMS-OPI dataset (Janowiak and Xie 1999). [Source: NOAA/NCDC.]

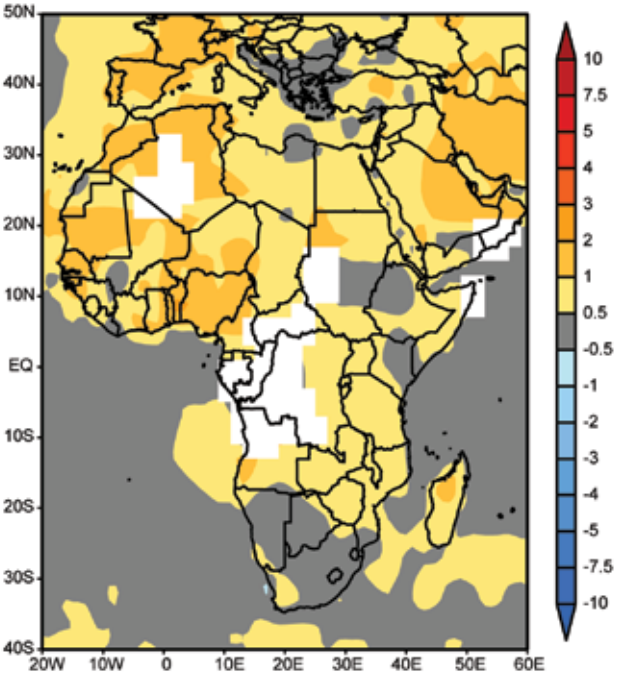

Fig. 6.2. African 2006 annual temperature anomalies (°C; 1971–2000 base) from CAMS-OPI.

decrease in Antarctic ozone depletion beginning around 2010, detectable at the 2σ level by 2023, and with a disappearance of the springtime ozone depletion phenomenon by 2070.

6. REGIONAL CLIMATES—A. Arguez, Ed.

a. Overview—A. Arguez

While a holistic (global) view of the 2006 state of the climate is a worthwhile vantage point, much can also be gleaned by analyzing individual continents, countries, and subregions. This section represents such a "downscaling" approach, as 2006 weather conditions over smaller geographic areas are not only described and put in a historical context, but international and interregional contrasts are also brought to light. The section is divided into seven sections: Africa, North America, Central America and the Caribbean, South America, Asia, Europe, and Oceania. These regions are further subdivided into practical climate divisions. Country and regional names utilized in this section do not, in any shape or form, reflect any political bias or sympathy. In addition, please note that varying base periods are often utilized for the computation of climate anomalies.

b. Africa—A. Arguez

Precipitation was generally above average over much of Sub-Saharan Africa in 2006 (Fig. 6.1). Several flood events and droughts occurred, causing substantial losses to human life and property. Most of Africa was slightly warmer than average for 2006 (Fig. 6.2). The following section discusses the state of the climate in four distinct regions: eastern Africa, northern Africa, southern Africa, and western Africa (including the Sahel).

1) Eastern Africa—M. Bell, C. Oludhe, P. Ambenje, L. Njau, Z. Mumba, and M. Kadi

The GHA countries have experienced heavy rainfall leading to severe flooding (the worst in the region for 50 years), causing loss of life and property in the region from October to November 2006. The worst hit were parts in Ethiopia, Somalia, and Kenya. Flood waters from the Juba River in Somalia and the Tana River in Kenya combined to inundate a large region of northeastern Kenya. Several rivers burst their banks, washing away roads and destroying bridges.

Climatologically, the timing of the rainy seasons in East Africa is governed by the meridional migration of the ITCZ through the course of the year. Although the complex orography and presence of the East African lakes make the climate of the region quite complicated, three general regimes can be delineated. In the southern sector, central and southern Tanzania has a unimodal rainfall regime, with precipitation primarily between December and April.